Becker, V.; Schwamm, T.; Urschel, S.; Antonino-Daviu, J. (2021). Fault Detection of Circulation Pumps on the Basis of Motor Current Evaluation. IEEE Transactions on Industry Applications. 57(5):4617-4624. https://doi.org/10.1109/TIA.2021.3085697

Fault Detection of Circulation Pumps on the Basis of Motor Current Evaluation

Vincent Becker, Thilo Schwamm, Sven Urschel, Jose Alfonso Antonino-Daviu

***Abstract* — Motor current signature analysis (MCSA) for fault detection has found widespread application, especially for induction motors (IM). The basis of MCSA is the evaluation of a motor's current. This analysis is now also used for other motor types and can be used to detect faults of the coupled load. The purpose of this paper is to examine whether MCSA can be used to detect faults in a wet-rotor pump. A total of three faults are examined. The results show that, compared to a healthy pump, all faults could be detected. However, a detailed analysis of frequency components has to be carried out to differentiate the faults. A circulation pump with a maximum power consumption of 1.1 kW was used as the test item.**

***Index Terms*—Permanent magnet motor, circulation pump, condition monitoring, motor current signature analysis, transient analysis, current, mechanical fault, impeller fault**

I. Introduction

Pumps are among the largest energy consumers in industry and in the household sector. Across the EU, pumps consume approximately 22 % of the electric motor energy in the industrial sector and 16 % in the services sector [1]. Circulation pumps alone, of which over 100 million are in operation, are responsible for about 2 to 3 % of the total electrical energy consumption in the EU [2]. The EU has recognized that increased efficiency can lead to major energy savings and thus CO_2 reduction. For this reason, the EU has adopted the ErP Directive (Energy related Products Directive), which specifies minimum efficiency levels, the so-called Energy Efficiency Index (EEI), for circulation pumps [3]. In order to meet the requirements of the EEI, today's circulation pumps are mostly designed as integrated wet-rotor pumps. This means that the process medium flows around the rotor of the electric motor. The wet rotor space is hermetically sealed from the dry stator space by a can [4]. The pump's impeller is in most cases driven by a permanent magnet synchronous motor (PMSM). With the help of the PMSM, energy efficiency can be achieved that cannot be achieved with an IM in the same installation space [5]. As the motor cannot be operated at the grid due to its principle, it is supplied via an integrated inverter, which also makes it possible to execute the control tasks.

The most common mode for controlling a circulation pump is proportional pressure control, where the head set point increases linearly with the flow [6]. Both flow and head are estimated by the pump based on the evaluation of the motor current. The motor current signal passes through an algorithm that includes both a pump and a motor model, and the hydraulic variables are calculated from this [7]. During the operation of a pump, however, the operating parameters change with increasing operating time due to wear or faults. According to the state of the art, this change in parameters is not considered in the implemented models [7]. Changed parameters can thus influence the control and therefore the energy efficiency of the pump. In addition to the usual advantages of predictive maintenance, such as cost savings and resource efficiency, a further objective is to adjust the model parameters to allow estimating the flow and the head. For this purpose, the faults have to be clearly identified first. Then it has to be possible to establish a connection between the fault and the model. In the context of this paper, the first step, fault identification, is investigated.

Typical mechanical faults can be divided into motor and hydraulic faults. In the context of a circulation pump, typical motor faults can be wear of the journal bearings, deformation of the can, dry-running, or calcification and contamination of the rotor space. Typical hydraulic faults are damage of the impeller, clogging of the impeller channels, or cavitation.

Since a circulation pump uses current sensors and a microprocessor unit by default, it provides a platform for current-based fault detection methods. Based on the assumption that only the motor current of the motor is evaluated, various methods for identifying motor faults have been developed, which are mainly used for IM. The best-known method is MCSA, which is based on the Fourier analysis of the current signal required by the motor in stationary operation [8]. In addition to faults that are typical for IM, such as broken rotor bars, mechanical faults that occur in all motor types are described in the literature. These faults include, above all, bearing damage [9] and eccentricities [10]. Meanwhile the MCSA is also successfully applied to detect faults in PMSM. It has been shown that both eccentricities [11], [12] and broken magnets [13] in PMSM can be detected by means of MCSA. Furthermore, the effect of the operation of a pump and its potential faults on the MCSA have also been analyzed [14].

With the aim of enabling even more reliable detection of faults, another method for investigating faults in motors has been developed. This approach is based on the analysis of the stator current during transient operation of a motor (Advanced Transient Current Signature Analysis, ATCSA) [15]. One

This work was supported by the German Federal Ministry for Economic Affairs and Energy within the framework 'Entwicklung optimierter Regelungen hydraulischer Systeme in der Gebäudetechnik zur Steigerung der Energieeffizienz von Heizungs- und Klimatisierungssystemen' (ref: 03ET1613B).

Vincent Becker is with the Kaiserslautern University of Applied Sciences, Schoenstrasse 11, 67657, Kaiserslautern, GERMANY (email:vincent.becker@hs-kl.de).

Thilo Schwamm is with the Kaiserslautern University of Applied Sciences, Schoenstrasse 11, 67657, Kaiserslautern, GERMANY (email: thilo.schwamm@hs-kl.de).

Sven Urschel is with the Kaiserslautern University of Applied Sciences, Schoenstrasse 11, 67657, Kaiserslautern, GERMANY (e-mail: sven.urschel@hs-kl.de).

Jose A. Antonino-Daviu is with the Instituto Tecnologico de la Energia, Universitat Politècnica de València, Camino de Vera s/n, 46022, Valencia, SPAIN (e-mail: joanda@die.upv.es)

possibility of implementing this approach is based on the analysis of the motor current during start-up using time-frequency transformations. The signal processing tools for ATCSA application can be based on discrete transforms or continuous transforms. The idea is to identify characteristic patterns caused by fault components during start-up in the time-frequency map [15]. Similar to MCSA, ATCSA is mainly applied to IM. One reason for this is the fact that an IM can be started on the grid. When starting up, the slip of the motor changes depending on the time. Faults that are dependent on slip then show a certain pattern in the analysis [16]. However, ATCSA is also applied for inverter-fed motors that perform a soft start-up [17].

This paper examines which faults of a circulation pump can be detected using these two approaches. The basis was presented in [18]. Three faults were provoked and measured on a pump test bench. The faults were a worn journal bearing, dry running of the rotor, and clogging of impeller channels. The motor current was measured in all cases and subsequently examined with the help of MCSA on the basis of a Fast Fourier Transformation and ATCSA on the basis of optimized continuous time-frequency transformations.

The structure of this paper is as follows. In Section II, the typical frequencies of PMSM that are influenced by mechanical faults are discussed. In Section III, the set-up and execution of the experiment is presented. The results of the MCSA and ATCSA of a healthy pump and three faulty configurations are discussed in Section IV. Section IV concludes this paper and provides a brief outlook on future work.

II. Fault Detection of Wet-rotor Pumps

Some faults have already been identified by different authors using MCSA and ATCSA. If electrical faults are excluded, three particular frequency components for wet-rotor pumps can be considered. From the literature it is known that problems with the bearings of the motor can lead to eccentricities of the rotor [8]. For this reason, eccentricities will be examined in more detail below. The pump impeller can also have an effect on the curve of the motor current [19]. Furthermore, a fault such as a broken blade can be visible in MCSA, as shown in [14], [20]. The theory of impeller faults will be described in the second part of this chapter.

A. Rotor Eccentricities

For eccentricities, a distinction is made between static, dynamic, and mixed eccentricity. Static eccentricity means that the rotor does not change its position during rotation. In the case of dynamic eccentricity, the rotor changes its position depending on its angle, with the rotor rotating around the center of the stator. Mixed eccentricity is a combination of static and dynamic eccentricity and the type of eccentricity that appears most often in practice [8].

Eccentricities cause amplitudes at certain frequencies of the current spectrum. Two families of frequency components are distinguished in the literature. The second frequency family results from the eccentricity caused by the rotor slots of IM [15]. As there are no slots in PMSM, the second frequency family is not applicable. For the influence of dynamic and static eccentricities on the frequency of the stator current, there is a general relationship for PMSM, given by equation 1 [21]. This equation is used to calculate the first family of eccentricity frequencies.

$$f_{ecc} = \left(n_{ws} \pm \frac{n_d}{p}\right) \cdot f_s \qquad (1)$$

Here, n_{ws} is the order of the stator harmonics (n_{ws}=1, 3, 5, …), f_s is the supply frequency of the stator current, n_d is the eccentricity order (n_d=0 (static eccentricity), 1, 2, …), and p is the number of pole pairs. This means that the only frequencies that are influenced by static eccentricity (n_d=0) are integer multiples of the stator frequency. The appearance of dynamic eccentricities depends on the number of pole pairs of the PMSM and the eccentricity order. The frequency components around the fundamental component (n_{ws}=1) are usually the most significant [21].

If the stator frequency is changed, the frequency component of the eccentricity also changes. This is of interest when considering start-up. The theoretical evolutions at the ramped start-up of the dynamic eccentricity components (n_{ws}=1, n_d=1) of an 8-pole PMSM are shown in Fig. 1. If there is dynamic eccentricity in a motor, the evaluation of the ATCSA should show an increased amplitude at the location of the red lines.

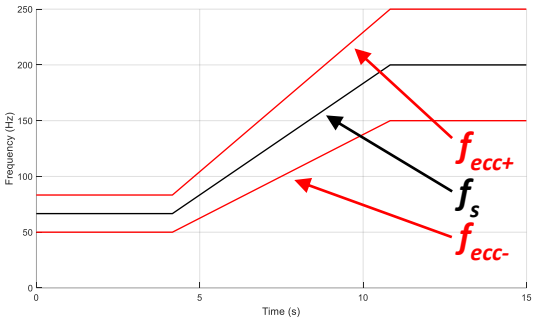

Fig. 1. Theoretical curves of the dynamic eccentricity components given by (1), for n_{ws}=1, n_d=1, for the start of an 8-pole PMSM (n_{start}=1000 rpm, n_{end}=3000 rpm)

B. Impeller Faults

The shaft power of a motor is converted into hydraulic power by means of an impeller. Since the impeller has a certain number of blades, a periodic vibration can be produced depending on the speed of the impeller. Every time the impeller is hydraulically loaded, the impeller produces an impulse. These oscillations are called blade pass frequency (BPF) vibration and can cause pressure pulsations in the pump [22]. If the amplitude is large, this can result in increased frequency sidebands in the stator current. Additionally, the BPF amplitude can indicate problems inside the pump, such as wear [20]. Equation 2 is used to calculate the BPF components. It applies to a motor without slip [19].

$$f_{BPF} = \left(1 \pm \frac{k_1 N_b}{p}\right) \cdot f_s \qquad (2)$$

Here, k_1 is a positive integer and N_b the number of blades.

Further problems of pumps, such as unbalance or misalignment, can occur in sidebands of the stator frequency depending on the speed; see equation 3 [20].

$$f_{r,pump} = \left(1 \pm \frac{1}{p}\right) \cdot f_s \qquad (3)$$

If equation 3 is compared with equation 1, it is noticeable that if n_{ws}=1 and n_d=1, f_{ecc} is equal to $f_{r,pump}$. In this case, the curve of $f_{r,pump}$, which is dependent on f_s, is similar to the curve shown in Fig. 1. This has to be taken into account when evaluating the results of MCSA and ATCSA.

III. Experiments

A circulation pump with a maximum power consumption of 1.1 kW and a nominal pipe size of DN 50 was tested. The functional principle is based on a wet-rotor pump driven by a PMSM. The motor is fed by an integrated inverter with a variable speed control of 1000 to 3000 rpm. Due to the high power of this pump, its field of application is mainly in heating systems of larger building complexes.

In the experiment, the rotor of the motor was equipped with eight permanent magnet excited poles. The stator winding was designed as a tooth coil winding with twelve slots. The impeller was designed as a radial impeller with seven blades. The shaft was supported by two journal bearings. A specially manufactured prototype was used as the can and split case (see Fig. 2). This allows the rotor to be removed from the can by loosening the screws. This is not possible with a standard version, as these spots are welded.

Fig. 2. The measured wet-rotor pump with a power of 1.1 kW.

The measurements were carried out on a pump test bench (see Fig. 3). The test bench consisted of a piping system connected to a reservoir. Pressure (WIKA DPT-10) and flow sensors (ABB Watermaster FER100) were used to measure the hydraulic values. A data acquisition system recorded the values of the sensors and controlled the actuators.

Fig. 3. The pump test bench.

The measurement setup shown in Fig. 4 ensured high-precision recording of the current signature. The three-phase current from the inverter induced an equivalent voltage signal in the zero flow current transducers (LEM IT 200-S), which were galvanically isolated from the power circuit. With the help of the Multichannel Current Transducer System (Signaltec MCTS), the supply of the current transducers was provided and their voltage signal was captured. The three galvanically isolated current channels and separate internal power supplies of the MCTS reduce both external and internal interference. The outgoing measuring signal was tapped via shunts (Yokogawa 19/SH5/BNC/0,05) and transmitted to the oscilloscope (Rhode & Schwarz RTE 1034). For each measurement, a sampling rate of 10 kHz with a running time of 60 s was set.

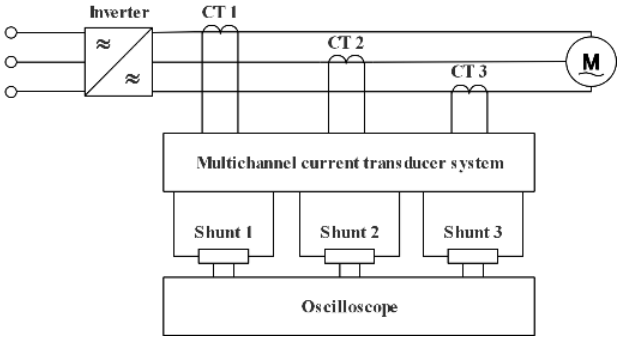

Fig. 4. Setup for precision measurement of the wet-rotor pump motor current.

To simulate real conditions, a flow of 10 m^3/h and a head of 11 m was set as the load point at a speed of 2800 rpm for the healthy pump. The valve position was kept constant during all measurements, both for stationary measurement and for start-up measurement. For the latter, the set speed of the PMSM was ramped up from 1000 to 3000 rpm.

In total, measurement was performed on four configurations. In addition to the healthy pump, three faults were provoked in the pump, which will be described in detail below.

A. *Worn Journal Bearing*

For wet-rotor pumps, the use of journal bearings is recommended. Materials for such bearings include rubber, carbon graphite, plastic, and wood. Over the lifetime of a pump, the journal bearings can wear out. The wear process is influenced by many factors, such as speed, load, or contamination of the lubricant.

The fault was provoked by grinding down a healthy journal bearing located in the metal housing (left side of Fig. 2) on the inside with the help of a lathe (see Fig. 5). This increased the inner diameter from 20 mm to 21 mm. The outer diameter of the journal bearing was 29 mm.

Fig. 5. Journal bearing of the wet-rotor pump.

B. *Dry Running of the Rotor*

The rotor of this type of wet-rotor pumps is normally surrounded by water. The water is mainly needed to lubricate the journal bearings. Without water, no lubricating film can

form between shaft and bearing. This can lead to increased heat development and wear of the journal bearings. The water enters the inside of the can via small holes and is pumped through the shaft, which is designed as a hollow shaft. If the water supply is stopped due to contamination, for example, the rotor can run dry. This fault was provoked with the help of foamed material and armor tape at the boreholes.

C. *Clogging of the Impeller Channels*

One type of faults that can occur in wet-rotor pumps is caused by contamination of the pumped medium. In this case, the channels of the impeller can become clogged. To test the effect of this fault on the measurement results, two of the seven channels were clogged with foam and armor tape (see Fig. 6). After the measurement, these spots were checked to see if the channels were still clogged.

Fig. 6. Impeller of the wet-rotor pump with two clogged channels.

IV. Results

The results of MCSA and ATCSA are presented below. The current spectrum is displayed in a range from 0 to 1000 Hz. The amplitude of the signal is normalized to the maximum value and is displayed in dB. In ATCSA, the frequency from 0 to 250 Hz is shown on the ordinate and the time from 0 to 15 or 20 s on the abscissa. For the healthy configuration, the range from 0 to 1000 Hz is also displayed.

A. *Healthy Condition*

In order to get a reference for considering the faults, the measurement results of the healthy pump will be considered first. Fig. 7 shows the MCSA of the stator current of one phase of the PMSM, while Fig. 8 and Fig. 9 show the ATCSA of the same phase for start-ups from 1000 to 3000 rpm.

The fundamental component can be seen at a frequency of 186.6 Hz in Fig. 7. Furthermore, considering Fig. 7 and Fig. 8, an increased amplitude can be seen at every integer multiple of the stator frequency. What is noticeable in Fig. 9 are some speed-independent components, especially at the 100 Hz and 10 Hz frequencies. A closer look at Fig. 8 reveals a component that starts at about 170 Hz and ends at 295 Hz, meaning it has a lower slope than all other components. These oscillations can be attributed to the design of the stator and the inverter operation. The component of the BPF of this configuration is at a frequency of 513.3 Hz (see equation 2) and is only weakly developed in the spectrum (-173 dB). If the frequency components around the stator frequency (3/4 and 5/4 times f_s) of a dynamic eccentricity are considered, a slight characteristic is noticeable. The amplitude of f_{ecc-} is -139 dB and that of f_{ecc+} is -154 dB. This result is also consistent with the result of the ATCSA; see Fig. 9. Here, a slight increase of the amplitude of f_{ecc-} is visible.

The results show that even in the healthy configuration, a very slight eccentricity can be detected.

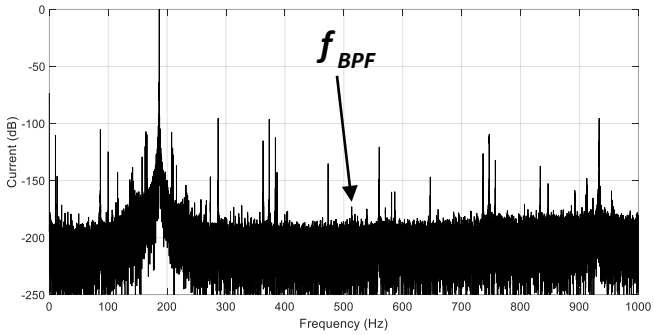

Fig. 7. MCSA of the wet-rotor pump in healthy condition at 2800 rpm.

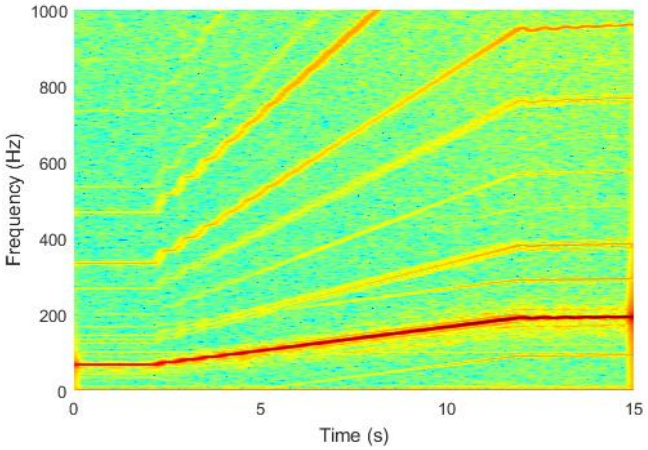

Fig. 8. ATCSA of the wet-rotor pump in healthy condition for a run-up from 1000 to 3000 rpm from 0-1000 Hz.

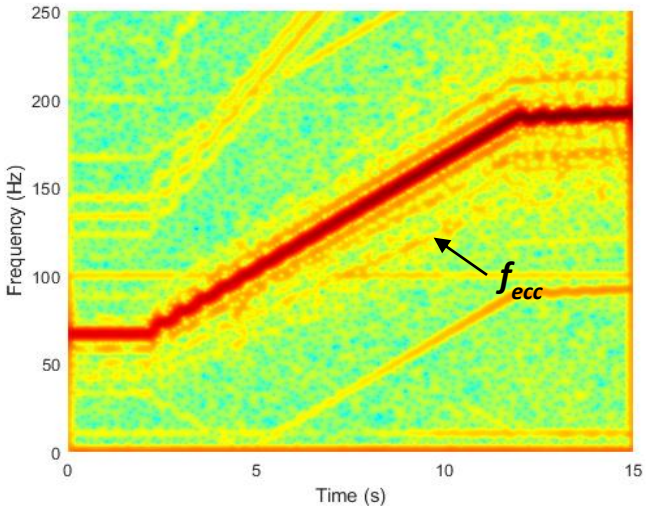

Fig. 9. ATCSA of the wet-rotor pump in healthy condition for a run-up from 1000 to 3000 rpm from 0-250 Hz.

B. *Worn Journal Bearing*

Fig. 10 depicts the MCSA and Fig. 11 the ATCSA of the pump with a worn journal bearing. Both figures show a significant amplitude of the sidebands around the stator frequency. Since the frequency components are at 3/4 and 5/4 times the stator frequency, they can be attributed to a dynamic eccentricity according to equation 1, for n_{ws}=1, n_d=1. Compared to the amplitude of the MCSA of the healthy pump, the component f_{ecc-} increases from -139 dB to -79 dB and f_{ecc+} increases from -154 dB to -93 dB. The ATCSA (Fig. 11) shows the typical color pattern for a motor with dynamic eccentricity, which is also shown in Fig. 1. It can be observed that this pattern only becomes visible once a certain speed is reached, about half-way through the run-up. What can also be

seen in Fig. 10 is an increase in the amplitude of the sidebands at the 5th harmonic (w_s=5). At 4.75 times of f_s (886.8 Hz), the amplitude increases from -185 dB to -130 dB, and at 5.25 times of f_s (980.2 Hz) from -193 dB to -129 dB compared to the healthy pump. These frequency components can be attributed to a dynamic eccentricity according to equation 1 (w_s=5, n_d=1). Due to the small absolute value of the amplitude, this frequency component is not visible in the ATCSA.

As described in chapter II. A. a static eccentricity should show an increase of amplitude at odd multiples of the fundamental components. At 3 times the basic frequency (560.1 Hz) as well as at 5 times (933.5 Hz), the amplitude remains about the same, compared to the healthy configuration (see Fig. 10).

These results are an indication that due to the worn journal bearing, the rotor no longer has any guidance and thus runs dynamically eccentrically.

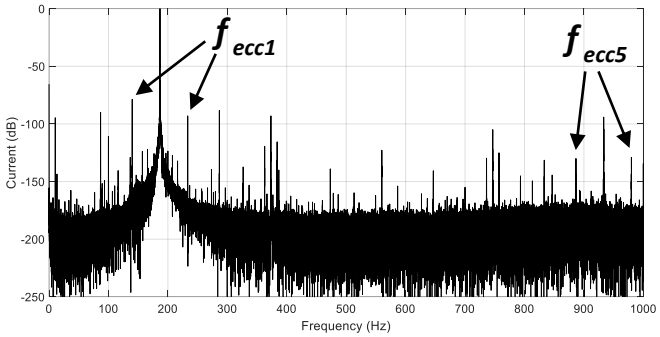

Fig. 10. MCSA of the wet-rotor pump with a worn journal bearing at 2800 rpm.

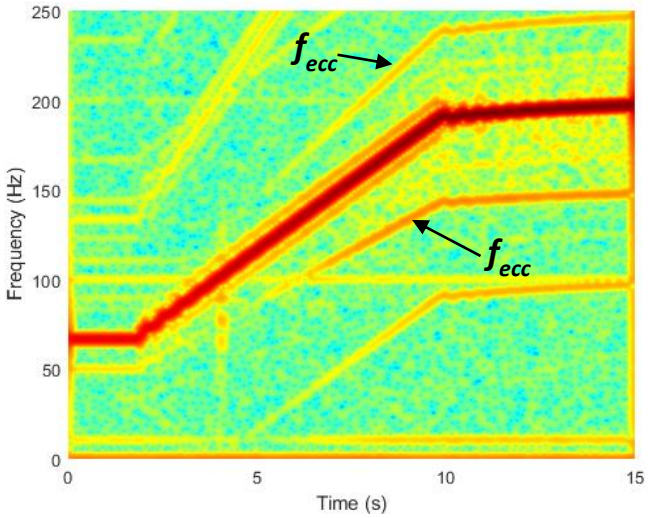

Fig. 11. ATCSA of the wet-rotor pump with worn journal bearings for a run-up from 1000 to 3000 rpm from 0-250 Hz.

C. *Dry-Running of the Rotor*

The MCSA and ATCSA results for the dry-running rotor are shown in Fig. 12 and Fig. 13, respectively. It can be seen from both analyses that the fault causes an increased amplitude of the dynamic eccentricity component. By comparing the MCSA of this fault (see Fig. 12) with the healthy configuration (see Fig. 7), the amplitude of f_{ecc-} increases from -139 dB to -113 dB and that of f_{ecc+} from -154 dB to -128 dB. The ATCSA (see Fig. 13) also shows the predicted pattern for dynamic eccentricity. Particularly notable is the f_{ecc-} component, which is visible over the entire time history. If the static eccentricity is considered (see equation (1), n_d=0), a slight reduction, from -121 dB to -130 dB, is noticeable at 3 times the stator frequency (560.1 Hz) compared to the healthy configuration. The amplitude of 5 times (933.5 Hz) the stator frequency remains the same in both configurations.

The results show that a slight dynamic eccentricity is caused by the dry-running rotor. This behavior can be explained by the fact that no lubricating film can form between the bearing and the shaft because there is no water in the rotor space. The gap between shaft and bearing is sufficient to cause a slight eccentricity.

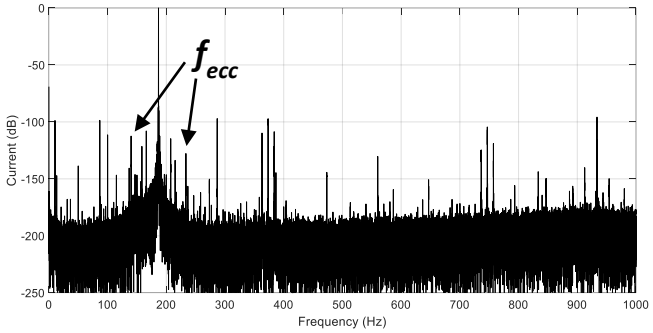

Fig. 12. MCSA of the wet-rotor pump with a dry-running rotor at 2800 rpm.

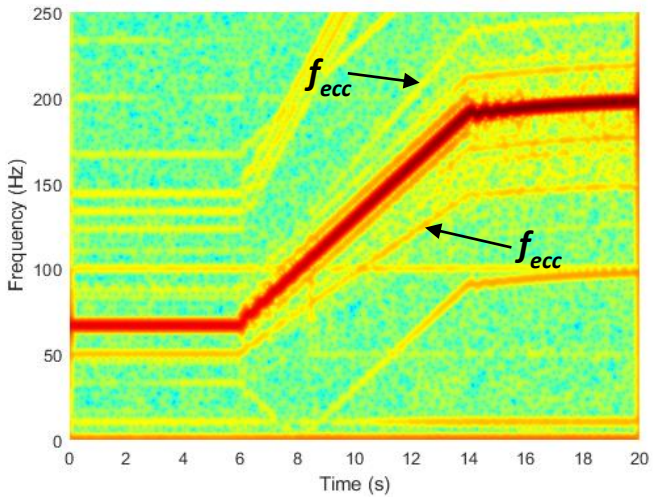

Fig. 13. ATCSA of the wet-rotor pump with a dry-running rotor for a run-up from 1000 to 3000 rpm from 0-250 Hz.

D. *Clogging of the Impeller Channels*

The MCSA and ATCSA results for the configuration with two clogged impeller channels are shown in Fig. 14 and Fig. 15, respectively. What is noticeable in both figures is the increase in amplitudes at the point of 3/4 and 5/4 times the stator frequency. In Fig. 15, the typical courses at these sideband frequencies are very noticeable. By comparing the MCSA of this fault (see Fig. 14) with the healthy configuration (see Fig. 7), the amplitude of the left sideband increases from -139 dB to -73 dB and that of the right sideband from -154 dB to -94 dB. Compared to the other two faults, these amplitudes are comparable to those of worn journal bearings. This fault is caused by the impeller and the frequency can be predicted using equation 3. What cannot be explained by equation 3, however, is the increase in the amplitudes of the sidebands around the 5th harmonic. This makes it difficult to distinguish this defect from a worn journal bearing. The clogging causes an imbalance, which is clearly visible in the stator current.

Since two of seven impeller channels cannot deliver hydraulic power, a look at the BPF makes sense. Compared to the healthy configuration, a slight increase of the BPF components at 513.3 Hz from -173 dB to -162 dB is observed. This increase is too small to conclude that a fault exists.

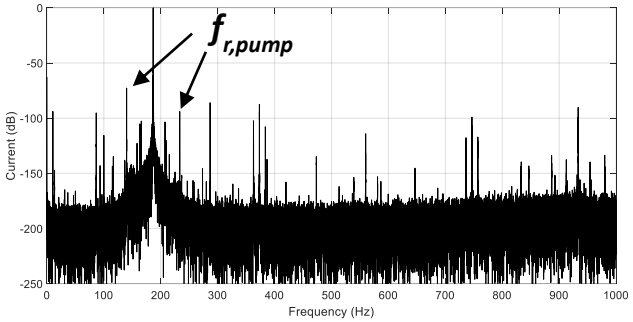

Fig. 14. MCSA of the wet-rotor pump with two clogged impeller channels at 2800 rpm.

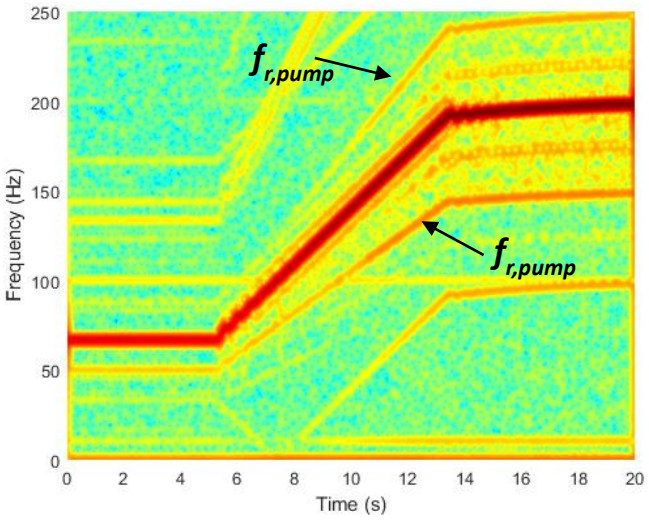

Fig. 15. ATCSA of the wet-rotor pump with two clogged impeller channels for a run-up from 1000 to 3000 rpm from 0-250 Hz.

E. Fault Separation

Summarizing the results presented in chapter IV. B. – IV. D. , all fault types cause an increase of the amplitudes at the frequencies where dynamic eccentricities occur. Considering equation 1, this is especially true for n_{ws}=1 and n_{ws}=5, where n_d=1. To differentiate between the faults, other features must therefore be considered.

Since the BPF component is not influenced by the faults, the only possibility based on chapter II. are the static eccentricity components. Based on equation 1 (n_d=0 for static eccentricities), the frequencies influenced by a static eccentricity are multiples of the stator frequency. The result of the MCSA of the healthy variant (see Fig. 7) shows that at every multiple of the stator frequency, a peak of different height is visible. This is why in the following every multiple is considered, and not only the odd multiples as mentioned in equation 1. Fig. 16 shows the amplitudes of the 2nd, 3rd, 4th, and 5th harmonic for the three phases of all three faults and for the healthy variant. It can be seen that the differences among the amplitudes are small. To avoid drawing wrong conclusions, the courses for all three phases are shown.

It can be observed that the curves vary from phase to phase. For example, the peak at the 3rd harmonic in phase 3 is significantly higher than the amplitudes of the other variants. In phase 1, the variants Healthy and Clogging have higher peaks. This shows that the analysis of a single phase could lead to false conclusions if the differences caused by a fault are small.

What is evident in all phases, however, is that due to the impeller clogging fault, the amplitudes at the 4th and 5th harmonics are the highest. In the place of the 4th harmonic, the amplitude is an average of 3.5 dB higher than the amplitude of the worn journal bearing fault and 4.5 dB higher than the amplitude of the dry-running fault. In the place of the 5th harmonic, the amplitude is an average of 4.1 dB higher than the amplitude of the worn journal bearing fault and 6.9 dB higher than the amplitude of the dry-running fault. The slightly higher differences and the higher absolute value of the 5th harmonic make it the best indicator for distinguishing the impeller clogging fault.

The amplitudes of the other variants are closer together. the amplitudes of the static eccentricity frequencies do not provide any added value for distinguishing the dry-running fault and the worn journal bearing fault from each other.

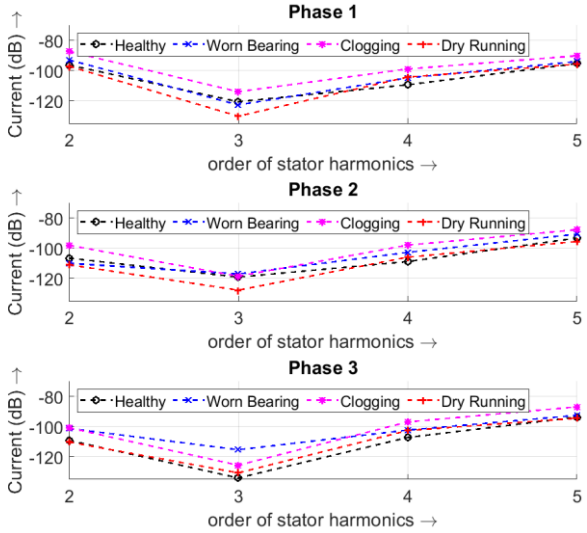

Fig. 16. Amplitudes of the harmonics of the stator current in MCSA for the three motor phases of all configurations

Another approach for separating the faults is the consideration of fault severity. The worn journal bearing fault in this paper is a severe fault as the radial bearing clearance is increased by 0.5 mm. With this bearing clearance, it can be assumed that dry friction will be present in the bearing. This results in increased bearing wear and thus increased bearing clearance in the case of further operation. If the sideband amplitudes around the stator frequency increase steadily, this could be an indication of bearing damage. If these amplitudes constantly increase with the same amplitude as in chapter IV. D. , this could indicate an impeller clogging fault. Further increased amplitudes that remain constant over time are also an indication of impeller clogging. In [23], it is shown that especially three and four adjacent clogged channels cause the highest increase of the amplitudes. This approach leads to additional questions that need to be answered. One question is at what point the bearing clearance becomes so large that dry friction occurs, which is a requirement for further bearing wear.

With the approaches presented in this paper, the dry-running fault cannot be separated from the other faults. Since

continuous dry running will result in bearing wear, the fault can be detected the latest at that time.

V. Conclusions

Three faults of wet-rotor pumps were examined in this paper. For each fault as well as for a healthy pump, both MCSA and ATCSA were performed. The implemented faults were a worn journal bearing, dry running of the rotor, and impeller clogging. All three faults showed a significant increase in the amplitudes of the stator frequency sidebands, at 3/4 and 5/4 times the stator frequency. Consequently, this frequency is an indicator that there is a mechanical fault, which can be important information for the pump operator.

For the exact identification of a fault, other frequencies have to be used. In particular, the worn journal bearing caused increased amplitudes at the sidebands around the 5th harmonic. However, the pump with clogged impeller channels also showed slightly increased amplitudes at these spots. This result indicates that there are additional frequency components caused by impeller clogging that are not predicted by the equation given in the literature. It was further demonstrated that the BPF for this type of pump showed only a weakly pronounced amplitude at the typical frequency components. The impeller clogging fault additionally caused a slightly higher increase of the amplitudes of the 4th and 5th harmonics than the other faults. Other approaches for fault separation include the consideration of the fault severity and the time courses of the amplitudes. These approaches were not addressed in detail here, as they will be the subject of future work.

In summary, the results show that the evaluation of the motor current of a wet-rotor pump can provide high added value. The findings of this paper can also be used to improve the interpretation of the MCSA and ATCSA of wet-rotor pumps. While MCSA has good potential for industrial implementation, ATCSA is mainly used for research into faults in this application. For the automated application of MCSA in a microprocessor, several approaches can be found in the literature [24]-[25]. An implementation of pump fault detection is part of future work.

VI. Acknowledgments

The authors would like to thank Dr. Martin Eckl and Dr. Stefan Laue of KSB for providing their support.

VII. References

[1] A. Almeida, P. Fonseca, H. Falkner and P. Bertoldi, “Market transformation of energy-efficient motor technologies in the EU,” Energy Policy. 2003. Pp. 563-575.

[2] S. Thomas, C. Barthel, Technology procurement for very energy efficient circulation pumps,” Final Report. Energy+ Pumps project. February 2009

[3] The European Parliament and the council of the European Union, “Directive 2009/125/EC of the European Parliament and of the Council”, October 2009

[4] S. Urschel and J. Dolgirev, "Energy- and resource saving synchronous reluctance machine for the use in circulation pumps," *2017 IEEE 3rd International Future Energy Electronics Conference and ECCE Asia (IFEEC 2017 - ECCE Asia)*, Kaohsiung, 2017, pp. 2139-2144.

[5] K. F. Rasmussen and N. Thorup, “Permanent Magnet Motors find their way to circulator pumps,” in Proceedings of the 3rd International Conference EEMODS'02 Energy Efficiency in Motor Driven Systems

[6] M. Eckl, F. Wurm, S. Liu, S. Urschel, J. Schullerer, J. Schaab and K. Kowalski, „New control mode to decrease energy consumption of circulator pumps” *4th International Rotating Equipment Conference*, Wiesbaden, 2019

[7] Method for the self-diagnosis of the mechanical and/or hydraulic state of a centrifugal pump, by M. Eckl and J. Schullerer. (2019, Jul. 25). *WO2019141658A1*. Accessed on: Jan. 6, 2019. [Online]. Available: https://patents.google.com/patent/WO2019141658A1/en

[8] W. T. Thomson and R. J. Gilmore, “Motor current signature analysis to detect faults in induction motor drive – fundamentals, data interpretation, and industrial case histories“, *Thirty-second Turbomachinery Symposium*, 2003

[9] M. El Hachemi Benbouzid, "A review of induction motors signature analysis as a medium for faults detection," in IEEE Transactions on Industrial Electronics, vol. 47, no. 5, pp. 984-993, Oct. 2000. J.R. Cameron,

[10] W.T. Thomson, “Vibration and current monitoring for detecting airgap eccentricity in large induction motors” *IEEE Proceedings*, Vol. 133, Pt. B, No. 3, May 1986, pp. 155-163.

[11] S. Rajagopalan, J. M. Aller, J. A. Restrepo, T. G. Habetler and R. G. Harley, "Detection of Rotor Faults in Brushless DC Motors Operating Under Nonstationary Conditions," in *IEEE Transactions on Industry Applications*, vol. 42, no. 6, pp. 1464-1477, Nov.-dec. 2006.

[12] J. Rosero, J. Cusido, J. A. Ortega, A. Garcia and L. Romeral, "On-line condition monitoring technique for PMSM operated with eccentricity," *2007 IEEE International Symposium on Diagnostics for Electric Machines, Power Electronics and Drives*, Cracow, 2007, pp. 95-100.

[13] W. le Roux, R. G. Harley and T. G. Habetler, "Detecting Rotor Faults in Low Power Permanent Magnet Synchronous Machines," in *IEEE Transactions on Power Electronics*, vol. 22, no. 1, pp. 322-328, Jan. 2007.

[14] K. Pradhan, P. & R. Mohanty, A. & N. P., M. & G. Dastidar, Sabyasachi. “Fault detection in a centrifugal pump using vibration and motor current signature analysis”. *International Journal of Automation and Control*. Volume 6, Nos. 3/4. ISSN 1740-7516 (electronic). 2012

[15] J. Antonino-Daviu and P. Popaleny, "Detection of Induction Motor Coupling Unbalanced and Misalignment via Advanced Transient Current Signature Analysis," *2018 XIII International Conference on Electrical Machines (ICEM)*, Alexandroupoli, 2018, pp. 2359-2364.

[16] J. A. Antonino-Daviu, M. Riera-Guasp, J. R. Folch and M. P. M. Palomares, "Validation of a new method for the diagnosis of rotor bar failures via wavelet transform in industrial induction machines," in IEEE Transactions on Industry Applications, vol. 42, no. 4, pp. 990-996, July-Aug. 2006.

[17] J. Pons-Llinares, D. Morinigo-Sotelo, O. Duque-Perez, J. Antonino-Daviu and M. Perez-Alonso, "Transient detection of close components through the chirplet transform: Rotor faults in inverter-fed induction motors," *IECON 2014 - 40th Annual Conference of the IEEE Industrial Electronics Society*, Dallas, TX, 2014, pp. 3386-3392.

[18] V. Becker, T. Schwamm, S. Urschel and J. A. Antonino-Daviu, "Detection of Rotor and Impeller Faults in Wet-rotor Pumps," 2020 International Conference on Electrical Machines (ICEM), Gothenburg, 2020, pp. 1308-1314, doi: 10.1109/ICEM49940.2020.9270767.

[19] Y. Park, M. Jeong, S. B. Lee, J. A. Daviu and M. Teska, "Influence of Blade Pass Frequency Vibrations on MCSA-Based Rotor Fault Detection of Induction Motors," in *IEEE Transactions on Industry Applications*, vol. 53, no. 3, pp. 2049-2058, May-June 2017.

[20] E. L . Bonaldi, J. G. B. da Silva, L. L. Oliveira and G. Lambert-Torres. “Predictive Maintenance by Electrical Signature Analysis to Induction Motors”

[21] S. Rajagopalan, W. l. Roux, T. G. Habetler and R. G. Harley, "Dynamic Eccentricity and Demagnetized Rotor Magnet Detection in Trapezoidal Flux (Brushless DC) Motors Operating Under Different Load Conditions," in *IEEE Transactions on Power Electronics*, vol. 22, no. 5, pp. 2061-2069, Sept. 2007.

[22] J. F. Gülich. „Centrifugal Pumps“, Springer Heidelberg Dordrecht London New York, ISBN 978-3-642-40113-8, 3rd Edition, 2014

[23] V. Becker, T. Schwamm, S. Urschel and J.A. Daviu, "Fault Investigation of Circulation Pumps to Detect Impeller Clogging" in Appl. Sci. 2020, 10, 7550

[24] S. M. A. Cruz, H. A. Toliyat and A. J. M. Cardoso, "DSP implementation of the multiple reference frames theory for the diagnosis of stator faults in a DTC induction motor drive," 4th IEEE International Symposium on Diagnostics for Electric Machines, Power Electronics and Drives, 2003. SDEMPED 2003., Atlanta, GA,USA, 2003, pp. 223-228, doi: 10.1109/DEMPED.2003.1234577.

[25] S. M. A. Cruz and A. J. M. Cardoso, "Multiple reference frames theory: a new method for the diagnosis of stator faults in three-phase induction motors," in IEEE Transactions on Energy Conversion, vol. 20, no. 3, pp. 611-619, Sept. 2005, doi: 10.1109/TEC.2005.847975.

VIII. BIOGRAPHIES

Vincent Becker received his B.Eng. in Energy Efficient Systems and his M.Eng. in Electrical Engineering from the Kaiserslautern University of Applied Sciences in 2015 and 2018, respectively. He has been working at the Kaiserslautern University of Applied Sciences in various research projects for three years. He is currently working towards his Ph.D. degree at the Kaiserslautern University of Applied Science in cooperation with Universitat Politècnica de València. His research interests include condition monitoring, efficient operation, and pump control.

Thilo Schwamm received his B.Eng. in Energy Efficient Systems from Kaiserslautern University of Applied Sciences and is currently studying to get his M.Eng. in Electrical Engineering from there. Since 2019 he is assistant at the Kaiserslautern University of Applied Science and has been working in various research projects. He is also the speaker of the university group of the German Association for Electrical Engineering, Electronics and Information Technologies Kurpfalz, Germany.

Sven Urschel received his German Diplom degree and his doctorate in Electrical Engineering, both from the Technical University Kaiserslautern, Germany, in 2003 and 2008, respectively. He worked for seven years for KSB AG in Frankenthal, Germany. There he was first a development engineer and later head of the Productionalisation department, where he was involved in various international projects. He is currently a full professor in the Department of Engineering at the Kaiserslautern University of Applied Sciences, Germany, where he carries out his teaching and research activities in the field of electrical machines, electrical drives, and magnetic fields. He heads the working group Electrotechnical Systems of Mechatronics and is the spokesperson for the research area Highly Efficient Technical Systems. He is also the deputy director of the Institute of Energy Efficient Systems and a member of the extended board of the German Association for Electrical, Electronic & Information Technologies Kurpfalz, Germany. He was a visiting professor at Dianji University Shanghai, China, in 2018 and 2019.

Jose A. Antonino-Daviu (S'04, M'08, SM'12) received his M.S. and Ph. D. degrees in Electrical Engineering, both from the Universitat Politècnica de València, in 2000 and 2006, respectively. He also received his B.S. in Business Administration from Universitat de Valencia in 2012. He worked at IBM for two years, where he was involved in several international projects. Currently, he is a full Professor in the Department of Electrical Engineering of Universitat Politècnica de València, where is engaged in lecturing and research work. He was a visiting professor at Helsinki University of Technology (Finland) in 2005 and 2007, Michigan State University (USA) in 2010, Korea University (Korea) in 2014, and Université Claude Bernard Lyon 1 (France) in 2015. He has been an IEEE Senior Member since 2012 and has published over 200 contributions in international journals, at conferences, and in books. He is also an Associate Editor of IEEE Transactions on Industrial Informatics and a former Guest Editor of IEEE Transactions on Industrial Electronics. Furthermore, he was General Co-Chair of IEEE SDEMPED 2013.